Validated numerical solutions for a semilinear elliptic equation on some topological annuli in the plane

Gianni Arioli [1] and Hans Koch [2]

Abstract. We consider the equation $-\Delta w = w^3$ with zero boundary conditions on planar domains that are conformal images of annuli. Starting with an approximate solution, we prove that there exist a true solution nearby. Our approach is computer-assisted. It involves simultaneous and accurate control of the (inverse) Dirichlet Laplacean, nonlinearities, and conformal mappings.

1. Introduction

We consider the boundary value problem

$$-\Delta w = w^3 \ \text{ on } \ \Omega\,, \qquad w = 0 \ \text{ on } \ \partial\Omega\,, \tag{1.1}$$

for a real-valued function w on a bounded doubly connected domain Ω in the plane.

It is well-known [4,11] that the equation $-\Delta w = |w|^{q-2}w$ on a bounded open domain in $d \geq 2$ dimensions with smooth boundary has an infinite number of distinct solutions for subcritical powers $2 < q < 2d/(d-2)$. Furthermore, if Ω is a ball $|z| < b$ or an annulus $a < |z| < b$ with $a > 0$, then there exist an infinite number of distinct solutions that are radial (depend on a point $z \in \Omega$ only via its distance from the origin $|z|$), and an infinite number of rotationally inequivalent non-radial solutions [9].

To obtain detailed information about solutions, the only approach available is often numerical. Numerical solutions to a variety of semilinear boundary value problems in $d = 2$ dimensions are described e.g. in [8,10]. When an interesting solution is observed numerically, it is natural to ask whether a true solution exists nearby. The method described in this paper allows us to answer such questions for some doubly connected domains in the plane. The square and the disk have been considered in [13,17].

Consider first an annular domain $a < |z| < b$ in the plane. Early results for this domain [5,6,7] established the existence of multiple positive solutions, with the number of rotationally inequivalent solutions tending to infinity as b/a approaches 1. The reason why such multiple solutions exist is best seen by characterizing nonzero solutions of (1.1) as critical points of a suitable functional J, such as

$$J(w) = \frac{\int_\Omega |\nabla w|^2}{\big[\int_\Omega w^4\big]^{1/2}}\,, \qquad w \in \mathrm{H}^1_0(\Omega)\,. \tag{1.2}$$

To be more precise, a nonzero solution w of the equation (1.1) corresponds to a line of critical points $t \mapsto tw$ of J. It is not hard to see that, for values of b/a close to 1, a minimizer of J cannot be radial. A single bump whose width is of the order $b-a$ can lead to a lower value of J. And by minimizing J in a subspace of functions $u \in \mathrm{H}^1_0(\Omega)$ that are

[1] Department of Mathematics, Politecnico di Milano, Piazza Leonardo da Vinci 32, 20133 Milano.

[2] Department of Mathematics, University of Texas at Austin, Austin, TX 78712

invariant under rotations by an angle $2\pi/k$, it is possible to find solutions with $k > 1$ local maxima, if b/a is sufficiently close to 1.

Figure 1 shows four solutions of this type, including a solution that has both positive and negative local extrema. A more precise description of these solutions is given below.

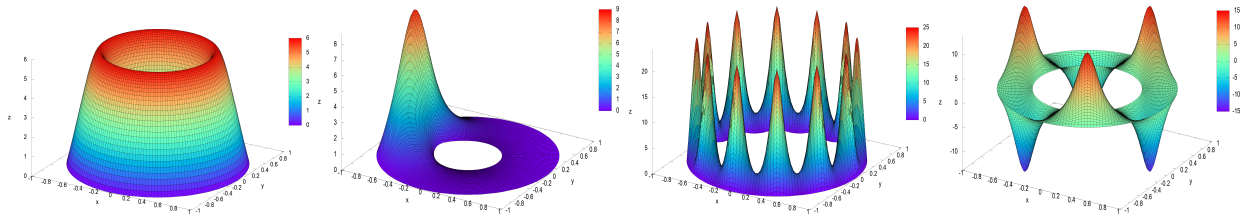

Figure 1. Solutions 1,2,3,4 on plain tori.

Other domains that admit multi-bump solutions are (for trivial reasons) disconnected domains. Consider e.g. a union of k mutually disjoint open disks, each containing a point from the unit circle. Such a domain can be made doubly-connected by taking its union with an annulus $1 - \varepsilon < |z| < 1 + \varepsilon$. It is well-known that stable multi-bump solutions persist on the resulting region Ω, if $\varepsilon > 0$ is chosen sufficiently small.

Similar solutions exist on topological annuli whose widths vary less drastically. Figures 2 and 3 show some solutions of this type. We note that the last solution in Figure 3, unlike its domain, has no symmetries. Identifying $\mathbb{R}^2$ with the complex plane $\mathbb{C}$, the domains used in Figures 2 and 3 are images of an annulus $A_\ell = \{\zeta \in \mathbb{C} : e^{-\ell} < |\zeta| < 1\}$ under a function $\psi_{\text{ex}} : A_\ell \to \mathbb{C}$ of the form

$$\psi_{\text{ex}}(\zeta) = \zeta - \frac{r}{n+1}\zeta^{n+1}\,, \qquad n \neq -1\,. \tag{1.3}$$

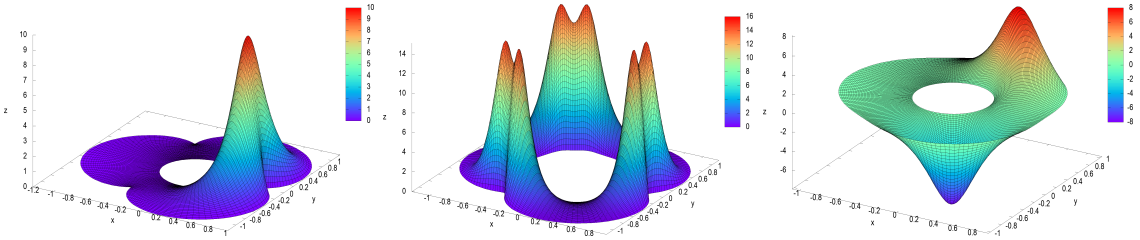

Figure 2. Solutions 5,6,7 on $\Omega_{\text{ex}} = \psi_{\text{ex}}(A_\ell)$, with $n = 3$.

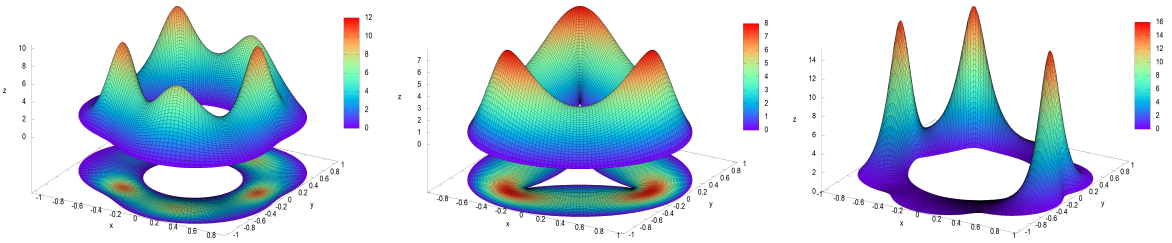

Figure 3. Solutions 8,9,10 on $\Omega_{\text{ex}} = \psi_{\text{ex}}(A_\ell)$, with $n = 3, -3, 6$.

The values of the parameters n, r, and ℓ that are used to define $\psi_{\rm ex}$ and A_ℓ are shown in Table 1. This table lists some other geometries and solutions that will be described below. It also includes the solutions depicted in Figure 1, which correspond to the choice $\psi_{\rm ann}(\zeta) = \zeta$. To simplify our descriptions, the solution described by the j-th row in Table 1 will be referred to as "solution j".

Remark 1. The 3d plots given in this section give a rather inaccurate picture of the domains. 2d plots of some of the domains $\Omega = \psi(A_\ell)$ and level sets for our solutions $w : \Omega \to \mathbb{R}$ can be found in Section 10, Figures 6,7,8,9.

Next, we describe some other domains that are images of A_ℓ under injective analytic mappings. Let D be the open unit disk in $\mathbb{C}$ and denote by $\bar D$ its closure. The mappings ψ considered here are analytic on an open neighborhood of $\bar D$. Substituting $w = v \circ \psi^{-1}$ into (1.1), we obtain the equation

$$-\Delta v = |\psi'|^2 v^3 \ \text{ on } \ A_\ell\,, \qquad v = 0 \ \text{ on } \ \partial A_\ell\,. \tag{1.4}$$

The most general conformal isomorphism of D is of the form $R_2 \circ \Psi_{\rm iso} \circ R_1$, where R_1 and R_2 are rotations about the origin, and where

$$\Psi_{\rm iso}(\zeta) = \frac{\zeta - r}{1 - r\zeta}\,, \qquad \psi_{\rm iso}(\zeta) = \big(1 - r^2\big)^{-2} \Psi_{\rm iso}(\zeta)\,, \tag{1.5}$$

with $-1 < r \le 0$. Here $\psi_{\rm iso}$ is a rescaled version of $\Psi_{\rm iso}$, which we prefer for our computations. Notice that the boundary of $\Omega_{\rm iso} = \psi_{\rm iso}(A_\ell)$ consists of two nested circles, which are non-concentric if $r \neq 0$.

Figure 4 depicts three solutions obtained for the domain $\Omega_{\rm iso}$. Intuitively, a minimizer w of J on a distorted annulus such as $\Omega_{\rm iso}$ has a single bump on a wide part of the domain. The reason is that rapid variations of w cause a large numerator in (1.2). Numerically, the Morse indices for the solutions 11,12, and 13 in Figure 4 are 1, 2, and 5, respectively. Here, the Morse index of a critical point w of J is defined to be one larger than the number of descending directions of J at w. We note that solutions 12 and 13 have descending directions that correspond to a "rotation" of these solutions. This seems typical for solutions that have bumps on narrow parts of the domain.

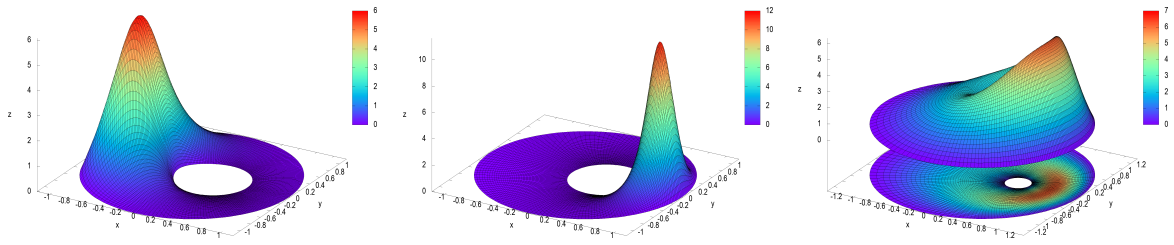

Figure 4. Solutions 11,12,13 on $\Omega_{\rm iso}$. Numerically, the indices are $1, 2, 5$.

Let us briefly comment on our procedure for finding approximate numerical solutions.

Each of the three solutions depicted in Figure 4 has been obtained by starting with a solution on the annulus, using $\psi_{\rm iso}$ with $r = 0$, and then following the solution as r is

being varied. The starting points for solutions 11 and 12 are single-bump solutions on the annulus. Solution 13 is a perturbation of the radial solution on the annulus that has (numerically) index 5. In all three cases, the perturbations was restricted to a subspace of functions w that are symmetric with respect to reflection about the horizontal axis. In this subspace, the indices of the three solutions are 1, 1, and 4, respectively, along the entire homotopy from $r = 0$ to the final values of r shown in Table 1. No bifurcations are encountered in these cases.

Solution 10 has no direct analogue on the annulus A_ℓ. It was constructed by placing bumps in the chosen places and iterating a contraction mapping of the type described in Section 7. The other solutions in Figures 2 and 3 have been obtained via homotopy from solutions on the annulus, by varying the value of the parameter r in the map ψ_{ex}. In particular, solution 8 is connected to a three-bump solution (at angles 0 and $\pm 2\pi/3$) on the annulus via two branches that are joined by a bifurcation.

Two other well-known planar domains are the inverted ellipse $\Psi_{\text{iel}}(D)$ defined by

$$\Psi_{\text{iel}}(\zeta) = \frac{2\alpha}{1+\alpha}\psi_{\text{iel}}(\zeta)\,, \qquad \psi_{\text{iel}}(\zeta) = \frac{\zeta}{1-r\zeta^2}\,, \qquad r = \frac{1-\alpha}{1+\alpha}\,, \tag{1.6}$$

and the Cassini oval $\Psi_{\text{cas}}(D)$ defined by

$$\Psi_{\text{cas}}(\zeta) = \sqrt{\frac{2\alpha}{1+\alpha}}\psi_{\text{cas}}(\zeta)\,, \qquad \psi_{\text{cas}}(\zeta) = \frac{\zeta}{\sqrt{1-r\zeta^2}}\,, \qquad r = \frac{1-\alpha}{1+\alpha}\,. \tag{1.7}$$

In both cases $0 < \alpha \le 1$. As $\alpha \to 0$, the region $\Psi(D)$ pinches down to zero on the imaginary axis. In the case of the Cassini oval, the limit domain is a figure eight with vertex at zero. In addition, we also consider the "near-Cassini oval" of order n. The corresponding mapping ψ_{ncs} is defined to be the Taylor polynomial of order $2n+1$ associated with ψ_{cas}.

Figures 5 depicts some solutions on $\Omega = \psi(A_\ell)$ with $\psi \in \{\psi_{\text{iel}}, \psi_{\text{cas}}, \psi_{\text{ncs}}\}$. The associated parameter values are listed in Table 1.

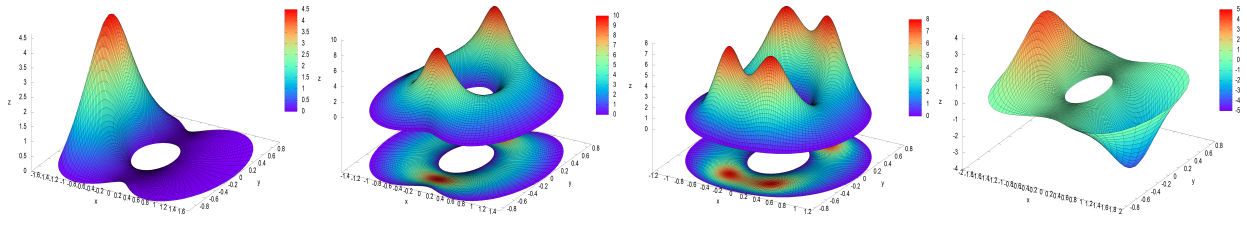

Figure 5. Solutions 14,15,16,17 on $\Omega = \psi(A_\ell)$, with $\psi = \psi_{\text{iel}}, \psi_{\text{iel}}, \psi_{\text{cas}}, \psi_{\text{ncs}}$.

The following result establishes the existence of the solutions mentioned above and describes some of their properties.

Theorem 1.1. *Consider the equation (1.1) associated with a fixed but arbitrary row of Table 1. The entry in column 5 specifies an annulus A_ℓ, and the entries in columns $2, 3, 4$ specify an injective mapping $\psi : A_\ell \to \mathbb{C}$. Then there exists a real analytic solution w*

of the equation (1.1) on $\Omega = \psi(A_\ell)$ with the following properties, described in rows 6–9 of Table 1. Column 6 indicates whether the solution is symmetric (+) or antisymmetric (−) under reflection about the horizontal axis. In column 7, a symbol ∞ stands for a radial solution, an integer $k > 1$ indicates a symmetry under a rotation by $2\pi/k$, and an integer $k < 0$ indicates an antisymmetry under a rotation by π/k. The absence of an entry in column 7 (6) means the absence of a rotation (reflection) symmetry. Column 8 lists the known positive local minima and negative local maxima, on a partition of the circle $\operatorname{range}(\arg\zeta)$ *into* 12 *arcs, as described below. And column 9 gives an interval that is contained in the range of w. Many more known properties of these solutions are described by our data in [20].*

Each of the solutions w mentioned in this theorem is close to an approximate solution $\bar{w}$ that has been found numerically. Our (computer-assisted) proof of Theorem 1.1 consists in verifying bounds on $\bar{w}$ that imply the existence of a true solution w near $\bar{w}$.

For some other computer-assisted proofs on boundary value problems in PDEs, we refer to [12,13,15,16,17] and references therein.

label	ψ	n	r	ℓ	ref	k	peaks	range	index
1	ann			1	+	∞		$(0, 5.8]$	~ 9
2	ann			1	+			$(0, 8.4]$	~ 1
3	ann			1/4	+	12		$(0, 24]$	~ 24
4	ann			1/2	+	−3		$[-13, 13]$	~ 6
5	ex	3	461/512	1	+			$(0, 9.7]$	~ 2
6	ex	3	3/4	1/2	+	3		$(0, 14]$	~ 9
7	ex	3	1/4	1	−			$[-7.9, 7.9]$	~ 2
8	ex	3	3/8	25/32	+			$(0, 10]$	~ 10
9	ex	−3	51/1024	1	+	3		$(0, 7.0]$	~ 9
10	ex	6	1/2	1/2				$(0, 14]$	~ 6
11	iso		−1/4	1	+			$(0, 5.8]$	~ 1
12	iso		−1/4	1	+			$(0, 11]$	~ 2
13	iso		−3/8	2	+			$(0, 6.0]$	~ 5
14	iel		13/32	1	+			$(0, 4.4]$	~ 1
15	iel		21/64	1	+	2		$(0, 9.8]$	~ 9
16	cas		11/32	1	+	2		$(0, 7.8]$	~ 8
17	ncs	50	3/4	1	+	−1		$[-4.0, 4.0]$	~ 2

Table 1. Parameter values and properties of solutions.

The last column in Table 1 shows the Morse index I of the solution. This result is purely numerical, whence the notation $\sim I$.

The vertical bars in the 8-th column labeled "peaks" represent a partition of the circle $\operatorname{range}(\arg\zeta)$ into 12 arcs $C_0, C_1, \ldots, C_{11}$. The angular interval C_k is centered at $k\pi/6$ and has width $\pi/6$. Each "high dot" on C_k represents a known positive local maximum of the solution, while each "low dot" represents a known negative local minimum. These extrema are "known" in the sense that they have been verified to exists. Numerically, there are no other local extrema, but we have not verified this. We note that, for our solutions 5–17, column 8 determines e.g. whether a local extremum is on a wide part of Ω or on a narrow part.

Remark 2. The information given in Table 1 is necessarily very incomplete. For each row in this table, we construct a small ball in a suitable Banach space that is centered at an approximate solution and encloses the true solution. Using this enclosure, it is possible to give rigorous upper and lower bounds on values, derivatives, and other quantities associated with the solution. In particular, many visible features in Figures 1-8 can be verified, if formulated in a precise way. (An example is our procedure `Horizontal_Values` [20] that determines upper and lower bounds on the extreme values on the lines $\arg\zeta = 0$ and $\arg\zeta = \pi$.) The necessary data and tools can be found in [20].

Results in the spirit of Theorem 1.1 have been obtained in [13,17] for equations of the type $-\Delta v = Wv^3$ on squares and disks. By choosing the weight function $W > 0$ carefully, it is possible e.g. to obtain solutions with fewer symmetries than what the domain and the weight W would allow. The equation (1.4) is of the same type; but $W = |\psi'|^2$ cannot be chosen ad-hoc, and the annular domain is harder to deal with than a square or a disk.

Using the methods given in [17], it would be relatively straightforward (albeit tedious) to prove that the Morse indices listed in Table 1 are correct. Additional work could include an analysis of solution branches and bifurcations, say as a function of our parameter $r \geq 0$. But this would go beyond the scope of the present paper.

The domains $\Omega = \psi(A_\ell)$ considered here are relatively tame, except for near-cusps with some choices of $\psi = \psi_{\text{ex}}$. More "distorted" annuli could be treated with similar methods, say $\psi \in \{\psi_{\text{iso}}, \psi_{\text{iel}}, \psi_{\text{cas}}\}$ with r closer to 1. But this makes the computation times for the proof uncomfortably large. The issue is that the factor $|\psi'|^2$ that appears in the equation (1.4) has to be controlled not only as a function, but as a multiplication operator on a suitable space of functions.

One of the main difficulties with computer-assisted proofs that involve infinite dimensional function spaces is to find a suitable expansion into "simple" functions. Our choice of expansion and spaces will be described in Section 3. Roughly speaking, we use Fourier series in both $\arg\zeta$ and $\log|\zeta|$. With this choice, the (inverse) Dirichlet Laplacean and products $v \mapsto v^3$ are relatively easy to control. What is less well behaved are multiplication operators like $v \mapsto |\psi'|^2 v$ that appear in the equation (1.4). Much of our analysis in this paper deals with this problem. The details are given in Sections 4, 5, and 8. Section 6 is devoted to the injectivity problem for ψ, especially for the near-Cassini map. In Section 7 we reduce the proof of Theorem 1.1 to concrete estimates that can be (and have been) verified with the aid of a computer. A sketch of the computer estimates is given in Section 9. The complete details of this part can be found in [20]. Section 10 contains some additional figures.

2. Functions on a cylinder

We parameterize the annulus A_ℓ by representing it as the image of the cylinder $\mathcal{C} = \mathbb{S} \times [0, \ell]$ under the exponential function $\phi(z) = e^{iz}$. Here, $\mathbb{S}$ denotes the circle $\mathbb{R}/(2\pi\mathbb{Z})$.

Substituting $v = u \circ \phi^{-1}$ into (1.4) leads to the equation

$$-\Delta u = |\Phi'|^2 u^3 \text{ on } \mathcal{C}\,, \qquad u = 0 \text{ on } \partial\mathcal{C}\,, \tag{2.1}$$

where $\Phi = \psi \circ \phi$. For $|\Phi'|$ we have by the chain rule

$$|\Phi'(z)| = |\psi'(\zeta)\phi'(z)| = |\psi'(\zeta)|e^{-y}\,, \qquad \zeta = e^{iz}\,, \quad z = x + iy\,. \tag{2.2}$$

A solution u of (2.1) also yields a solution $w = u \circ \Phi^{-1}$ for the original equation (1.1).

Given a real number $\rho > 1$, denote by $\mathcal{B}$ the space of all real analytic functions $h : \mathbb{S} \to \mathbb{R}$ that admit a Fourier series representation with a finite norm $\|h\|$,

$$h(x) = h_0 + \sum_{m=1}^{\infty} \Big[h_m \cos(mx) + h_{-m} \sin(mx)\Big]\,, \quad \|h\| = \sum_{m=-\infty}^{\infty} |h_m| \frac{\rho^m + \rho^{-m}}{2}\,. \tag{2.3}$$

Here, $h_m \in \mathbb{R}$ for all integers m. Notice that $\mathcal{B}$ is a Banach algebra under pointwise multiplication of functions.

Denote by $\mathcal{D}$ the subspace of all functions $h \in \mathcal{B}$ whose second derivatives h'' belong to $\mathcal{B}$ as well. For every positive integer n, define $\Delta_n : \mathcal{D} \to \mathcal{B}$ by setting

$$\Delta_n h = h'' - (n\pi/\ell)^2 h\,, \qquad h \in \mathcal{D}\,. \tag{2.4}$$

Clearly Δ_n has a compact inverse $\Delta_n^{-1} : \mathcal{B} \to \mathcal{B}$.

In connection with symmetries, we also consider the following subspaces of $\mathcal{B}$. Given an integer $k \geq 2$, the subspace of all functions $u \in \mathcal{B}$ with the property that $u_m = 0$ whenever $m \not\equiv 0 \pmod{k}$ will be denoted by $\mathcal{B}_k$. For $k \geq 1$, the subspace of all functions $u \in \mathcal{B}$ with the property that $u_m = 0$ whenever $m \not\equiv k \pmod{2k}$ will be denoted by $\mathcal{B}_{-k}$. For $k = \infty$ we define $\mathcal{B}_k$ to be the set of all constant functions on $\mathbb{S}$. The subspace of all even functions in $\mathcal{B}$ or $\mathcal{B}_k$ will be denoted by $\mathcal{B}^+$ or $\mathcal{B}_k^+$, respectively. And the subspace of all odd functions in $\mathcal{B}$ or $\mathcal{B}_k$ will be denoted by $\mathcal{B}^-$ or $\mathcal{B}_k^-$, respectively. Notice that all these subspaces are invariant under Δ_n^{-1}.

Let $\mathcal{X}$ be any Banach algebra with unit. Give a positive real number τ, denote by $\mathcal{A}_\mathcal{X}$ the space of all functions $u : [0, \ell] \to \mathcal{X}$ that admit the following expansion and have a finite norm $\|u\|$,

$$u(y) = \sum_{n=1}^{\infty} u_n \sin(n\kappa y)\,, \qquad \|u\| = \sum_{n=1}^{\infty} \|u_n\|(1 + \tau n)\,, \qquad u_1, u_2, \ldots \in \mathcal{X}\,, \tag{2.5}$$

where $\kappa = \pi/\ell$. Notice that a function $u \in \mathcal{A}_\mathcal{X}$ is of class C^1 and vanishes at the endpoints of $[0, \ell]$. Furthermore, $u \mapsto u^3$ maps $\mathcal{A}_\mathcal{X}$ into itself.

$\mathcal{A}_\mathcal{B}$ can be identified with a space of functions $u : \mathcal{C} \to \mathbb{R}$. This space will be used in our construction of solutions for the equation (2.1). A function $u = u(x, y)$ in $\mathcal{A}_\mathcal{B}$ is of class C^1 on $\mathcal{C}$ and real analytic in the variable $x \in \mathbb{S}$. Furthermore, it vanishes on $\partial\mathcal{C}$.

The Laplacean Δ is defined on a dense subspace of $\mathcal{A}_\mathcal{B}$ and has a compact inverse $\Delta^{-1} : \mathcal{A}_\mathcal{B} \to \mathcal{A}_\mathcal{B}$ given by the equation $(\Delta^{-1}u)_n = \Delta_n^{-1}u_n$. So the equation (2.1) for a function $u \in \mathcal{A}_\mathcal{B}$ can be written as a fixed point equation $G(u) = u$, where

$$G(u) = -\Delta^{-1}|\Phi'|^2 u^3\,. \tag{2.6}$$

Remark 3. As mentioned above, every function $u \in \mathcal{A}_{\mathcal{B}}$ is of class C^1. If u is a fixed point of G, then u is of class C^∞ by elliptic regularity. So $w = u \circ \Phi^{-1}$ is of class C^∞ as well. Given that $-\Delta w = w^3$ on Ω, this in turn implies that w is real analytic on Ω [1,2,19].

We note that our expansion (2.5) represents a compromise: rapid convergence is sacrificed in favor of simple properties of the modes $(x, y) \mapsto \cos(mx)\sin(nky)$ and $(x, y) \mapsto \sin(mx)\sin(nky)$ with respect to products and the inverse Laplacean. Alternative choices involve Zernike functions or Bessel function in the radial direction. Zernike functions can yield exponential convergence on the disk [17], but imposing boundary conditions on the inner circle of ∂A_ℓ reduces this to ℓ^2 convergence in general. And Bessel functions lead to slow convergence in the linearization of products.

Remark 4. The derivative $DG(u)$ for $u \in \mathcal{A}_{\mathcal{B}}$ defines a compact positive self-adjoint linear operator on $\mathrm{H}^1_0(\mathcal{C})$. It is not hard to show that, if u is a fixed point of G, then the Morse index of $w = u \circ \Phi^{-1}$ agrees with the number of eigenvalues of $DG(u)$ of modulus larger that 1; see also [17]. Computing these eigenvalues numerically yields the indices in the last column of Table 1.

3. The determinants $|\Phi'|^2$

The transformation G defined by (2.6) is composed of the nonlinear map $u \mapsto u^3$, the multiplication operator $u \mapsto |\Phi'|^2 u$, and the negative inverse Laplacean $-\Delta^{-1}$. On the space $\mathcal{A}_{\mathcal{B}}$ considered here, both $u \mapsto u^3$ and $-\Delta^{-1}$ are quite easy to control. So let us describe the multiplication operators in more detail.

Recall from (2.2) that $|\Phi'(z)| = |\psi'(\zeta)|e^{-y}$, where $\zeta = e^{iz}$ and $z = x + iy$, with $x \in \mathbb{R}$ and $y \in [0, \ell]$. In the example (1.3), we have

$$\bigl|\psi'_{\mathrm{ex}}(\zeta)\bigr|^2 = 1 - 2r\cos(nx)e^{-ny} + r^2 e^{-2ny}\,. \tag{3.1}$$

This simple example already highlights a difficulty with Fourier series in the variable y: the k-th Fourier coefficient of the function $y \mapsto e^{-y}$ on $[0, \ell]$ decreases only like k^{-2}.

For the disk-isomorphism (1.5), the determinant of the derivative is given by

$$\bigl|\psi'_{\mathrm{iso}}(\zeta)\bigr|^2 = |1 - r\zeta|^{-4} = F_{1,\infty}(x, y)^2\,, \tag{3.2}$$

where

$$F_{k,N}(x, y) \stackrel{\text{def}}{=} \sum_{m,n=0}^{N} r^{n+m}\cos(k(n-m)x)e^{-k(n+m)y} \qquad (N \le \infty)\,, \tag{3.3}$$

for all positive integers k. The convergence of this series and similar ones will be discussed in the next section. For the inverted ellipse (1.6), we have

$$\bigl|\psi'_{\mathrm{iel}}(\zeta)\bigr|^2 = \left|\frac{1 + r\zeta^2}{\bigl(1 - r\zeta^2\bigr)^2}\right|^2 = \Bigl[1 + 2r\cos(2x)e^{-2y} + r^2 e^{-4y}\Bigr] F_{2,\infty}(x, y)^2\,. \tag{3.4}$$

And the determinant for the Cassini oval (1.7) is given by

$$\left|\psi'_{\rm cas}(\zeta)\right|^2 = \left|(1-r\zeta^2)\right|^{-3} = H_\infty(x,y)\,, \tag{3.5}$$

where

$$H_N(x,y) \stackrel{\rm def}{=} \sum_{n,m=0}^{N} C_n C_m r^{n+m}\cos((n-m)x)e^{-(n+m)y} \qquad (N\le\infty) \tag{3.6}$$

and

$$C_n = (-1)^n\binom{-3/2}{n} = \prod_{k=1}^{n}\frac{2k+1}{2k}\,. \tag{3.7}$$

Finally, for the near-Cassini map of finite order N, we have $|\psi'_{\rm ncs}(\zeta)|^2 = H_N(x,y)$.

In all these cases, multiplication by $|\Phi'(z)|^2 = |\psi'(z)|^2 e^{-2y}$ is an operator of the form

$$\mathbb{L} = \sum_{q=0}^{\infty}\hat{h}_q L^q\,, \qquad (Lu)(y) \stackrel{\rm def}{=} e^{-y}u(y)\,, \tag{3.8}$$

where $\hat{h}_q$ is multiplication by a function $h_q\in\mathcal{B}$. The multiplication operators $\hat{h}_q$ are easy to control, due to the fact that $\mathcal{B}$ is a Banach algebra. So let us now consider powers of L.

4. The operator L

A straightforward computation shows that

$$(L^q u)_j = \sum_{n=1}^{\infty} L^q_{j,n}u_n\,, \qquad j=1,2,\dots \tag{4.1}$$

for every $q\neq 0$, with

$$L^q_{j,n} = K_{n-j}(q)\left[\frac{1}{(n-j)^2+(q/\kappa)^2} - \frac{1}{(n+j)^2+(q/\kappa)^2}\right]. \tag{4.2}$$

The functions K_n in this equation, and functions Σ_n that will be needed below, are given by

$$K_n(q) = \frac{q}{\ell\kappa^2}\left[1-e^{-q\ell}(-1)^n\right], \qquad \Sigma_n(q) = \sum_{k\ge n}\frac{1}{k^2+(q/\kappa)^2}\,. \tag{4.3}$$

Notice that the two terms in the difference $[\dots]$ in (4.2) nearly cancel for large values of n. This is the main reason behind the following fact.

Lemma 4.1. *L defines a bounded linear operator on $\mathcal{A}$ for every choice of $\tau>0$. Furthermore, there exists a constant $B_\tau\le 4$, with $B_\tau\to 2$ as $\tau\to 0$, such that for all $q\neq 0$,*

$$\|L^q\| \le K_1(q)\big[\Sigma_0(q) + B_\tau\Sigma_1(q)\big]\,. \tag{4.4}$$

For relatively small values of q, we estimate $\Sigma_n(q)$ with $n \in \{0,1\}$ by computing $\Sigma_n(q) - \Sigma_m(q)$ explicitly for some large value of m and then using that

$$\Sigma_m \leq \sum_{k=m}^{\infty} \frac{1}{k^2 - \frac{1}{2}} = \sum_{k=m}^{\infty} \left[\frac{1}{k - \frac{1}{2}} - \frac{1}{k + \frac{1}{2}} \right] = \frac{1}{m - \frac{1}{2}}\,, \qquad m \geq 1\,. \tag{4.5}$$

But in order estimate the tail of operator series like (3.8), we need a bound on $\|L^q\|$ for arbitrarily large $q > 0$.

Define

$$\varrho_p(L) = \sup_{q \geq p} \|L^q\|^{1/q}\,, \qquad p \geq 1\,. \tag{4.6}$$

Clearly, the sequence $p \mapsto \varrho_p(L)$ is decreasing, and its limit is the spectral radius $\varrho(L)$ of the operator $L : \mathcal{A} \to \mathcal{A}$.

Proposition 4.2. *$\varrho(L) = 1$, and*

$$\varrho_p(L) \leq K_1(p)^{1/p} \max\bigl(\Sigma_0(p) + B_\tau \Sigma_1(p), 1\bigr)^{1/p}\,, \qquad p > e\ell\kappa^2\,. \tag{4.7}$$

Proof. Since $q \mapsto \bigl[1 + e^{-ql}\bigr]^{1/q}$ is decreasing and $x \mapsto x^{1/x}$ is decreasing for $x > e$, the sequence $q \mapsto K_1(q)^{1/q}$ is decreasing for $q > e\ell\kappa^2$. Let $f(q) = \max\bigl(\Sigma_0(q) + B_\tau \Sigma_1(q), 1\bigr)$. This defines a decreasing function $f \geq 1$.

Let $q \geq p > e\ell\kappa^2$. Then by Lemma 4.1, we have

$$\|L^q\|^{1/q} \leq K_1(q)^{1/q} f(q)^{1/q} \leq K_1(q)^{1/q} f(p)^{1/q} \leq K_1(p)^{1/p} f(p)^{1/p}\,. \tag{4.8}$$

This proves (4.7). Since $K_1(p)^{1/p} \to 1$ as $p \to \infty$, we have $\varrho(L) \leq 1$. And the definition $(Lu)(y) = e^{-y} u(y)$ of L shows that $\varrho(L) \geq 1$. Thus, $\varrho(L) = 1$ as claimed. **QED**

5. Bounds on the factors $|\psi'|^2$

The function H_N given by (3.6) defines a multiplication operator $\mathbb{H}_N$ of the type (3.8), acting on the space $\mathcal{A}_\mathcal{B}$. Similarly, the function $F_{k,N}$ given by (3.3) defines a multiplication operator $\mathbb{F}_{k,N}$. They are well defined for $N < \infty$. The goal here is to control the limit $N \to \infty$.

Recall that these operators depend on a parameter $r \in (-1, 1)$. To simplify notation, let us assume that r is nonnegative. Denote by $\rho > 1$ the weight used in the definition (2.3) of the norm on the space $\mathcal{B}$. The following propositions will be used with $\rho_\circ \geq \varrho_{N+1}(L)$.

Proposition 5.1. *Let $k, N \geq 1$. Let $\rho_\circ > 1$ be such that $r\rho_\circ^{2k} < 1$. Assume that $\rho < \rho_\circ$ and $\|L^q\| \leq \rho_\circ^q$ for $q > N$. Then $\mathbb{F}_{k,\infty}$ defines a bounded linear operator on $\mathcal{A}_\mathcal{B}$, and*

$$\|\mathbb{F}_{k,\infty} - \mathbb{F}_{k,N}\| \leq f_{N+1}\bigl(r\rho_\circ^{2k}\bigr) f_0(r) + f_0\bigl(r\rho_\circ^{2k}\bigr) f_{N+1}(r)\,, \tag{5.1}$$

where $f_m(t) = \sum_{n=m}^{\infty} t^n = t^m(1-t)^{-1}$ *for all* $m \geq 0$.

The proof of this proposition is analogous to to the proof of the following.

Proposition 5.2. *Let* $N \geq 1$. *Let* $\rho_\circ > 1$ *be such that* $r\rho_\circ^4 < 1$. *Assume that* $\rho < \rho_\circ$ *and* $\|L^q\| \leq \rho_\circ^q$ *for* $q > N$. *Then* $\mathbb{H}_\infty$ *defines a bounded linear operator on* $\mathcal{A}_\mathcal{B}$, *and*

$$\|\mathbb{H}_\infty - \mathbb{H}_N\| \leq h_{N+1}\big(r\rho_\circ^4\big)h_0(r) + h_0\big(r\rho_\circ^4\big)h_{N+1}(r)\,, \tag{5.2}$$

where $h_m(t) = \sum_{n=m}^{\infty} C_n t^n$ *for all* $m \geq 0$. *In particular,* $h_0(t) = (1-t)^{-3/2}$.

Proof. Let $E_N = \|\mathbb{H}_\infty - \mathbb{H}_N\|$. Using the definition (3.6) of H_N and the fact that $\mathcal{B}$ is a Banach algebra, we have

$$\begin{aligned} E_N &\leq \sum_{n\vee m>N} C_n C_m r^{n+m}\, \frac{\rho^{2(n-m)} + \rho^{2(m-n)}}{2}\, \rho_\circ^{2(n+m)} \\ &\leq \sum_{n\vee m>N} C_n C_m r^{n+m}\, \frac{\rho_\circ^{4n} + \rho_\circ^{4m}}{2} = \sum_{n\vee m>N} C_n C_m r^{n+m} \rho_\circ^{4n} \\ &\leq \sum_{n>N} C_n r^n \rho_\circ^{4n} \sum_{m\geq 0} C_m r^m + \sum_{n\geq 0} C_n r^n \rho_\circ^{4n} \sum_{m>N} C_m r^m \\ &= h_{N+1}\big(r\rho_\circ^4\big)h_0(r) + h_0\big(r\rho_\circ^4\big)h_{N+1}(r)\,, \end{aligned} \tag{5.3}$$

where $n \vee m = \max(m,n)$. Given that $\mathbb{H}_N$ is bounded for all positive integers N, the assertion follows. **QED**

In order to get a useful bound on the functions h_m that appear in Proposition 5.2, we first need the following.

Proposition 5.3. *If* $n \geq N$, *then* $\dfrac{C_n}{C_N} \leq \sqrt{\dfrac{n+1/2}{N+1/2}}$.

Proof. Clearly, the given bound holds for $n = N$. If $n > N$, then

$$\frac{C_n^2}{C_N^2} = \prod_{N<k\leq n} \left(\frac{2k+1}{2k}\right)^2 < \prod_{N<k\leq n} \frac{2k+1}{2k}\,\frac{2k}{2k-1} = \prod_{N<k\leq n} \frac{2k+1}{2k-1} = \frac{2n+1}{2N+1}\,, \tag{5.4}$$

where we have used the identity (3.7). **QED**

Proposition 5.4. *Let* $0 \leq t < 1$. *Then* $h_m(t) = \sum_{n=m}^{\infty} C_n t^n$ *satisfies the bound*

$$h_m(t) \leq C_m t^m \frac{1}{1-t}\left(1 + \frac{1}{2m+1}\cdot\frac{t}{1-t}\right). \tag{5.5}$$

.

Proof. We use the summation by parts formula

$$\sum_{n=m}^{k} u_n v'_n = (u_k v_{k+1} - u_m v_m) - \sum_{n=m}^{k-1} v_{n+1} u'_n \,, \qquad \begin{matrix} u'_n = u_{n+1} - u_n \,, \\ v'_n = v_{n+1} - v_n \,, \end{matrix} \tag{5.6}$$

where $k \geq m \geq 0$. Setting $u_n = C_n$ and $v_n = t^n$, we have

$$u'_n = C_n \left(\frac{C_{n+1}}{C_n} - 1 \right) = \frac{1/2}{n+1} C_n \,, \qquad v'_n = -(1-t)t^n \,. \tag{5.7}$$

Notice that $u_k v_{k+1} \to 0$ as $k \to \infty$. Using (5.6) and Proposition 5.3, we obtain

$$\begin{aligned} (1-t) \sum_{n=m}^{\infty} C_n t^n &= - \sum_{n=m}^{\infty} u_n v'_n = C_m t^m + \frac{1}{2} \sum_{n=m}^{\infty} t^{n+1} \frac{1}{n+1} C_n \\ &\leq C_m t^m + \frac{1}{2} C_m \sum_{n=m}^{\infty} t^{n+1} \frac{1}{n+1} \sqrt{\frac{n+\frac{1}{2}}{m+\frac{1}{2}}} \\ &\leq C_m t^m + \frac{1}{2m+1} C_m \sum_{n=m}^{\infty} t^{n+1} \leq C_m t^m + \frac{1}{2m+1} C_m \frac{t^{m+1}}{1-t} \\ &= C_m t^m \left(1 + \frac{1}{2m+1} \cdot \frac{t}{1-t} \right) . \end{aligned} \tag{5.8}$$

This implies the bound (5.5). **QED**

6. Injectivity of the maps ψ

Part of the claim in Theorem 1.1 is that $\psi : A_\ell \to \mathbb{C}$ is injective. This is obvious for $\psi_{\rm ann}$. It is well-known for $\psi = \psi_{\rm iso}$ with $|r| < 1$, and for $\psi \in \{\psi_{\rm iel}, \psi_{\rm cas}\}$ with $0 \leq r < 1$. In these cases, ψ is in fact injective on the unit disk D. For $\psi_{\rm ex}$ defined by (1.3), we have the following.

Proposition 6.1. *If $n > 0$ and $|r| < 1$, or if $n < -1$ and $|r| < e^{n\ell}$, then $\psi_{\rm ex}$ is injective on the annulus A_ℓ.*

A proof of this proposition is a straightforward computation.

Injectivity of the near-Cassini map $\psi_{\rm ncs}$ of order N cannot easily be checked by hand. Here we will use the following.

Proposition 6.2. *The near-Cassini map $\psi_{\rm ncs}$ of order N is injective if the following two inequalities hold:*

$$(1+r) \frac{2r^{N+1}}{1-r} \leq 1 \,, \qquad \frac{1+r^2}{1-r} \left[\frac{1}{(1-r)^{1/2}} \, h_{N+1}(r) + \frac{r^{N+1}}{(1-r)^2} \right] \leq 1 \,, \tag{6.1}$$

where $m \mapsto h_m$ is the sequence of functions described in Proposition 5.4.

A proof of this proposition will be given below.

The following is a well-known consequence of the Jordan curve theorem and the argument principle. Assume that ψ is analytic on an open neighborhood of the closed unit disk $\bar{D}$.

Proposition 6.3. *ψ is one-to-one on $\bar{D}$ if and only if ψ is one-to-one on ∂D.*

Consider now the restriction of ψ to ∂D. Write $\zeta = e^{ix}$ and $\psi(\zeta) = re^{i\vartheta}$, with x, r, ϑ real. Our goal is to show that $\frac{\partial \vartheta}{\partial x}$ has no zeros on ∂D. This implies that ψ is n-to-one on ∂D for some $n > 0$. A straightforward computation shows that $\frac{\partial \vartheta}{\partial x} = \mathrm{Re}\big(\zeta\psi'/\psi\big)$. Thus, let us consider

$$\chi(\zeta) \stackrel{\text{def}}{=} \mathrm{Re}\Big[\zeta\psi'(\zeta)\overline{\psi(\zeta)}\Big]\,. \tag{6.2}$$

Proposition 6.3 implies the following.

Corollary 6.4. *Assume that $\psi(\zeta) = \psi(1)$ holds only if $\zeta = 1$. Assume furthermore that ψ and χ do not vanish on ∂D. Then ψ is one-to-one on D.*

Proof of Proposition 6.2. It suffices to verify the assumptions of Corollary 6.4 for $\psi = \psi_{\mathrm{ncs}}$. This can be done by comparing ψ_{ncs} to the Cassini mapping ψ_{cas}. By (1.7) we have

$$\psi_{\mathrm{cas}}(\zeta) = \zeta\big(1 - r\zeta^2\big)^{-1/2}\,, \qquad \zeta\psi'_{\mathrm{cas}}(\zeta) = \zeta\big(1 - r\zeta^2\big)^{-3/2}\,. \tag{6.3}$$

Expanding these functions in powers of r and restricting to $\zeta = e^{ix}$ with $x \in \mathbb{R}$ yields

$$\psi_{\mathrm{cas}}(e^{ix}) = \sum_{m=1}^{\infty} B_m r^m e^{(2m+1)ix}\,, \qquad e^{ix}\psi'_{\mathrm{cas}}(e^{ix}) = \sum_{n=1}^{\infty} C_n r^n e^{(2n+1)ix}\,, \tag{6.4}$$

where $B_n = (-1)^m\binom{-1/2}{m}$ and $C_n = (-1)^n\binom{-3/2}{n}$. The corresponding expressions for the near-Cassini approximation of order N are obtained by restricting the above sums to $m \le N$ and $n \le N$, respectively. This leads to the expressions

$$E_\psi \stackrel{\text{def}}{=} \big|\psi_{\mathrm{cas}}(e^{ix})\big|^2 - \big|\psi_{\mathrm{ncs}}(e^{ix})\big|^2 = \sum_{m\vee n > N} B_m B_n r^{m+n}\cos(2(n-m)x) \tag{6.5}$$

and

$$E_\chi \stackrel{\text{def}}{=} \chi_{\mathrm{cas}}(e^{ix}) - \chi_{\mathrm{ncs}}(e^{ix}) = \sum_{m\vee n > N} B_m C_n r^{m+n}\cos(2(n-m)x)\,, \tag{6.6}$$

where $m \vee n = \max(m, n)$.

Notice that the sequence $n \mapsto B_n$ is decreasing. This yields a bound

$$\sum_{n>N} B_n r^n = \sum_{k\ge 0} B_{N+1+k} r^{N+1+k} \le r^{N+1}\sum_{k\ge 0} B_k r^k = \frac{r^{N+1}}{(1-r)^{1/2}}\,. \tag{6.7}$$

So E_ψ can be estimated as

$$E_\psi \le 2 \sum_{m\ge 0} B_m r^m \sum_{n>N} B_n r^n \le \frac{2}{(1-r)^{1/2}} \frac{r^{N+1}}{(1-r)^{1/2}} = \frac{2r^{N+1}}{1-r} \,. \tag{6.8}$$

And for E_χ we have

$$\begin{aligned} E_\chi &\le \sum_{m\ge 0} B_m r^m \sum_{n>N} C_n r^n + \sum_{m>N} B_m r^m \sum_{n\ge 0} C_n r^n \\ &\le \frac{1}{(1-r)^{1/2}}\, h_{N+1}(r) + \frac{r^{N+1}}{(1-r)^{1/2}} \frac{1}{(1-r)^{3/2}} \\ &= \frac{1}{(1-r)^{1/2}}\, h_{N+1}(r) + \frac{r^{N+1}}{(1-r)^2} \,. \end{aligned} \tag{6.9}$$

Now we can use the upper bounds

$$\left|\psi_{\rm cas}(e^{ix})\right|^2 \ge \frac{1}{1+r} \,, \qquad \chi_{\rm cas}(e^{ix}) \ge \frac{1-r}{(1+r)^3} \,, \tag{6.10}$$

which easily follow from (6.3).

Combining (6.8) with the first inequality in (6.10), we have

$$\left|\psi_{\rm ncs}(e^{ix})\right|^2 = \left|\psi_{\rm cas}(e^{ix})\right|^2 - E_\psi \ge \frac{1}{1+r} - \frac{2r^{N+1}}{1-r} \,. \tag{6.11}$$

Thus, in order to guarantee that $\psi_{\rm ncs}$ does not vanish on ∂D, it suffices that the right hand side of (6.11) is positive. This condition is equivalent to the first inequality in (6.1).

Combining (6.9) with the second inequality in (6.10), we have

$$\chi_{\rm ncs}(e^{ix}) = \chi_{\rm cas}(e^{ix}) - E_\chi \ge \frac{1-r}{(1+r)^3} - \left[\frac{1}{(1-r)^{1/2}}\, h_{N+1}(r) + \frac{r^{N+1}}{(1-r)^2} \right] . \tag{6.12}$$

Thus, in order to guarantee that $\chi_{\rm ncs}$ does not vanish on ∂D, it suffices that the right hand side of (6.12) is positive. This condition is equivalent to the second inequality in (6.1).

Finally, we note that $|\psi_{\rm ncs}(e^{ix})| < \psi_{\rm ncs}(1)$ if $e^{ix} \ne 1$. This follows from the fact that $C_n > 0$ for all n. Having shown that the conditions (6.1) imply the hypotheses of Corollary 6.4, our proof of Proposition 6.2 is complete. **QED**

7. Solution of the fixed point equation

Here we reduce the proof of Theorem 1.1 to specific estimates. Consider the equation (2.1) associated with a fixed but arbitrary row of Table 1, say row j. The symmetry entries in columns 6 and 7 specify a subspace $\mathcal{A}_j$ of $\mathcal{A}_\mathcal{B}$. To be more precise, a value k in column 7 defines $\mathcal{A}_j = \mathcal{A}_{\mathcal{B}_k}$ or $\mathcal{A}_j = \mathcal{A}_{\mathcal{B}_k^\pm}$, depending on whether column 6 is empty or lists one of

"±", respectively. The absence of an entry in column 7 defines $\mathcal{A}_j = \mathcal{A}_{\mathcal{B}}$ or $\mathcal{A}_j = \mathcal{A}_{\mathcal{B}^\pm}$, respectively. Here, $\mathcal{B}^\pm$, $\mathcal{B}_k$, and $\mathcal{B}_k^\pm$ are the subspaces of $\mathcal{B}$ defined in Section 2.

Assume for now that the transformation G given by (2.6) is well-defined on $\mathcal{A}_j$.

As is common in many computer-assisted proofs, we associate with G a quasi-Newton map $\mathcal{N}$ as follows. Given a function $\bar{u} \in \mathcal{A}_j$ and a bounded linear operator M on $\mathcal{A}_j$, define

$$\mathcal{N}(h) = G(\bar{u} + Ah) - \bar{u} + Mh\,, \qquad A = \mathrm{I} - M\,, \tag{7.1}$$

for every $h \in \mathcal{A}_j$. Clearly, if h is a fixed point of $\mathcal{N}$, then $\bar{u} + Ah$ is a fixed point of G.

Our goal is to apply the contraction mapping theorem to the map $\mathcal{N}$, acting on a ball $B_\delta = \{h \in \mathcal{A}_j : \|h\| < \delta\}$. Thus, $\bar{u}$ is chosen to be an approximate fixed point of G.

Lemma 7.1. *Consider the equation (2.1) associated with a fixed but arbitrary row of Table 1, say row j. The entry in column 5 specifies an annulus A_ℓ, and the entries in columns $2, 3, 4$ specify an injective mapping $\psi : A_\ell \to \mathbb{C}$. Let $\Phi = \psi \circ \phi$. Then there exists domain parameters $\rho > 1$ and $\tau > 0$ such that the following holds for the associated space $\mathcal{A}_j$. The multiplication operator $u \mapsto |\Phi'|^2 u$ defines a bounded linear operator on $\mathcal{A}_j$. So the equation (2.6) defines a compact cubic map G on $\mathcal{A}_j$. Furthermore, there exists a function $\bar{u} \in \mathcal{A}_j$, a bounded linear operator M on $\mathcal{A}_j$, and a real number $\delta > 0$, such that the map $\mathcal{N}$ defined by (7.1) satisfies bounds*

$$\|\mathcal{N}(0)\| \le \varepsilon\,, \qquad \|D\mathcal{N}(h)\| \le K\,, \qquad \forall h \in B_\delta\,, \tag{7.2}$$

with $\varepsilon, K > 0$ satisfying $\varepsilon + K\delta < \delta$. Let $u = \bar{u} + Ah$ with $h \in B_\delta$ arbitrary. Then u has precisely the symmetries described in columns 6 and 7 of Table 1. Moreover, the range of u includes the interval in column 9. Furthermore, $v = u \circ \psi^{-1}$ has a set of extrema as described in column 8.

Our proof of this lemma is computer-assisted and will be described in Section 9.

Lemma 7.1 implies Theorem 1.1. Namely, the contraction mapping theorem guarantees that $\mathcal{N}$ has a fixed point $h \in B_\delta$. The associated function $u = \bar{u} + Ah$ is a fixed point of G. Thus, $w = u \circ \Phi^{-1}$ is a solution of the equation (1.1) on the domain $\Omega = \Phi(\mathcal{C})$. It is real analytic, for the reasons described in Remark 3. The properties of w described in columns 6–9 of Table 1 follow from the last three statements in Lemma 7.1.

8. Estimates for the operator L

Recall from (2.5) that a function $u \in \mathcal{A}$ admits a unique representation $u = \sum_{j\ge1} u_j \sigma_j$ with $\sigma_j(y) = \sin(j\kappa y)$. For $q \neq 0$ define

$$L_-^q u = \sum_{\substack{n,j\ge1\\ j\le n}} L_{j,n}^q u_n \sigma_j\,, \qquad L_+^q u = \sum_{\substack{n,j\ge1\\ j>n}} L_{j,n}^q u_n \sigma_j\,, \qquad u \in \mathcal{A}\,. \tag{8.1}$$

The following two propositions imply Lemma 4.1.

Proposition 8.1. *L^q_- defines a bounded linear operator on $\mathcal{A}$, and $\|L^q_-\| \le K_1(q)\Sigma_0(q)$.*

Proof. Using the expression in (4.2) for the coefficients $L^q_{j,n}$ that appear in the definition (8.1), we have

$$\|L^q_-\| = \sup_n \sum_{j\le n} K_{n-j}(q) \left[\frac{1}{(n-j)^2+(q/\kappa)^2} - \frac{1}{(n+j)^2+(q/\kappa)^2}\right] \frac{1+\tau j}{1+\tau n}\,, \tag{8.2}$$

with the right hand side being possibly infinite. An upper bound is obtained by dropping the second term in $[\ldots]$. Since $0 < K_n(q) \le K_1(q)$ for all n and $\frac{1+\tau j}{1+\tau n} \le 1$ for $j \le n$, we have

$$\|L^q_-\| \le K_1(q) \sup_n \sum_{j\le n} \frac{1}{(n-j)^2+(q/\kappa)^2} \le K_1(q)\Sigma_0(q)\,, \tag{8.3}$$

and the claim of Proposition 8.1 follows. **QED**

Proposition 8.2. *L^q_+ defines a bounded linear operator on $\mathcal{A}$. Furthermore, there exists a constant $B_\tau \le 4$, with $B_\tau \to 2$ as $\tau \to 0$, such that $\|L^q_+\| \le B_\tau K_1(q)\Sigma_1(q)$.*

Proof. From (4.2) we have

$$L^q_{j,n} = K_{n-j}(q) \frac{4nj}{((n-j)^2+(q/\kappa)^2)((n+j)^2+(q/\kappa)^2)}\,. \tag{8.4}$$

Thus,

$$\|L^q_+\| = \sup_n \sum_{j>n} K_{n-j} \frac{4nj}{((j-n)^2+(q/\kappa)^2)((j+n)^2+(q/\kappa)^2)} \frac{1+\tau j}{1+\tau n}\,. \tag{8.5}$$

Since $0 < K_n(q) \le K_1(q)$ for all n and $\frac{1+\tau j}{1+\tau n} \le \frac{j}{n}$ whenever $j > n$, we find that

$$\begin{aligned}
\|L^q_+\| &\le 4K_1(q) \sup_n \sum_{j>n} \frac{nj}{((j-n)^2+(q/\kappa)^2)((j+n)^2+(q/\kappa)^2)} \frac{1+\tau j}{1+\tau n} \\
&\le 4K_1(q) \sup_n \sum_{j>n} \frac{j^2}{((j-n)^2+(q/\kappa)^2)((j+n)^2+(q/\kappa)^2)} \\
&\le 4K_1(q) \sup_n \sum_{j>n} \frac{1}{(j-n)^2+(q/\kappa)^2} = 4K_1(q)\Sigma_1(q)\,.
\end{aligned} \tag{8.6}$$

This show that $\|L^q_+\| \le B_\tau K_1(q)\Sigma_1(q)$ with $B_\tau \le 4$.

Notice that the first sum in (8.6) is a continuous function of $\tau \ge 0$, and continuity is uniform in q. So consider (8.5) for $\tau = 0$. Then the bound $nj\frac{1+\tau j}{1+\tau n} \le j^2$ used in (8.6) can be replaced by $nj \le \frac{1}{2}(j+n)^2$. As a result we obtain $\|L^q_+\| \le 2K_1(q)\Sigma_1(q)$. This shows that $\|L^q_+\| \le B_\tau K_1(q)\Sigma_1(q)$ with $B_\tau \to 2$ as $\tau \to 0$. **QED**

If we think of L^q as a matrix $(j,n) \mapsto L^q_{j,n}$, then L^q_- represents the upper triangular part of L^q, while L^q_+ represents the strictly lower triangular part. In our computer-assisted

proofs, this matrix is being subdivided further into "blocks". Each such block is characterized by additional restrictions on the index pair (j,n). This allows us to improve bounds such as (8.3) and (8.6).

To be more specific, we represent a function $u \in \mathcal{A}$ by a finite number of "coefficient modes" $\mathbb{P}_j u$ and (bounds on) a finite number of "error modes" $\mathbb{P}_{\geq d} u$, where

$$\mathbb{P}_j u = u_j \sigma_j \,, \qquad \mathbb{P}_{\geq d} u = \sum_{j \geq d} u_j \sigma_j \,, \qquad u = \sum_{j \geq 1} u_j \sigma_n \,, \tag{8.7}$$

with $\sigma_j(y) = \sin(j\kappa y)$. Naturally, the estimates in Propositions 8.1 and 8.2 can be improved when considering $\mathbb{P}_{\geq d} L^q_\pm \mathbb{P}_n$ in place of $L^q_\pm$. In particular, if $n \leq d$, then we have a bound $\|\mathbb{P}_{\geq d} L^q \mathbb{P}_n\| \leq B_\tau K_1(q) \Sigma_{d-n}(q)$. Another useful bound concerns the operator $L^q_{-\nu} = \sum_{n>\nu} \mathbb{P}_{n-\nu} L^q \mathbb{P}_n$ with $\nu \geq 0$. A straightforward computation show that $\|L^q_{-\nu}\| \leq K_\nu(q) / \bigl(\nu^2 + (q/\kappa)^2\bigr)$.

9. Computer estimates

The estimates that are necessary to prove Lemma 7.1 are carried out with the aid of a computer. This part of the proof is written in the programming language Ada [21] and can be found in [20]. The following is meant to be a rough guide for the reader who wishes to check the correctness of our programs.

9.1. Enclosures and data types

Bounds on a vector x in a space $\mathcal{X}$, also referred to as enclosures for x, are given here by sets $X \subset \mathcal{X}$ that include x and are representable as data on a computer. The enclosure associated with data `B` will be denoted by $\mathtt{B}_{\mathcal{X}}$. Our basic data type `Ball` consists of a pair `B` = (`B.C`, `B.R`), where `B.C` is a representable number [23] and `B.R` a nonnegative representable number (type `Radius`). If $\mathcal{X}$ is a Banach algebra with unit $\mathbf{1}$, then $\mathtt{B}_{\mathcal{X}} = \{x \in \mathcal{X} : \|x - (\mathtt{B.C})\mathbf{1}\| \leq \mathtt{B.R}\}$. Other types of enclosures depend on the algebra $\mathcal{X}$. At a level where details are irrelevant, we use an unspecified type `Scalar`.

Given an integer $D > 0$, data of type `CpCosSin1` consist of a triple `U=(U.P,U.C,U.E)`, where `U.P` $\in \{0,1\}$, `U.C` is an `array (0 .. D) of Scalar`, and `U.E` is an `array (0 .. 2*D) of Radius`. The type `CpCosSin1` is used to define enclosures in the space $\mathcal{A}_{\mathcal{X}}$. The enclosure $\mathtt{U}_{\mathcal{A}}$ associated with `U` is the set of all functions

$$u = \sum_{j=p}^{D} u_j \sigma_j + \sum_{j=p}^{2D} e_j \,, \qquad p = \mathtt{U.P} \,, \tag{9.1}$$

with u_j belonging to $\mathtt{U.C(j)}_{\mathcal{X}}$, and with $e_j \in \mathbb{P}_{\geq j} \mathcal{A}_{\mathcal{X}}$ having norm $\|e_j\| \leq \mathtt{U.E(j)}$. To be more precise, the space $\mathcal{A}_{\mathcal{X}}$ defined earlier only allows odd functions (`E.P=1`). In this case $\sigma_j(y) = \sin(j\kappa y)$. Here, we also allow even functions (`E.P=0`), where $\sigma_j(y) = \cos(j\kappa y)$. For details we refer to the Ada package `CpCosSins1`.

In our application, we use the above mostly with $\mathcal{X} = \mathcal{B}$. In this case, `CpCosSins1` is instantiated with `Scalar => Fourier1`, where `Fourier1` is the data type used to define

enclosures in $\mathcal{B}$. The precise definition of the type `Fourier1` and the associated enclosures is given in the Ada package `Fouriers1`. We will not give more detail here, since the same type has been described and used in earlier work [14].

Consider now bounded linear operators $\mathbb{L} : \mathcal{A}_\mathcal{X} \to \mathcal{A}_\mathcal{X}$ of the type (3.8). If $\hat{h}_q$ denotes multiplication by $h_q \in \mathcal{X}$, then we set $\|\mathbb{L}\|_\mathcal{L} = \sum_q \|h_q\| \|L^q\|$. This defines a Banach space $\mathcal{L}_\mathcal{X}$. Our enclosures for this space are associated with the type `LTaylors`. Data of this type are pairs `T=(T.C,T.E)`, where `T.C` is an `array(0 .. d) of Scalar` and `T.E` is a `Radius`. The enclosure represented by `T` is the set of all operators $\mathbb{L} = \sum_q \hat{h}_q L^q$ with $h_q \in$ `T.C(q)`$_\mathcal{X}$ for $q \le d$, and with $\left\|\sum_{q>d} \hat{h}_q L^q\right\|_\mathcal{L} \le$ `T.E`. For details we refer to the package `LTaylors`. We only use this type for $\mathcal{X} = \mathcal{B}$, in which case `LTaylors` is instantiated with `Scalar => Fourier1`.

We use some other data types and enclosures, but they are trivial compared to the ones described above. This includes vectors in $\mathcal{X}^n$ and matrices in $\mathcal{X}^{n\times n}$, with enclosures of type `Vector` and `Matrix`, respectively, based on arrays of `Scalar`.

9.2. Bounds and procedures

When working with enclosures, a bound on a map $f : \mathcal{X} \to \mathcal{Y}$ is a function F that assigns to a set $X \subset \mathcal{X}$ of a given type (`Xtype`) a set $Y \subset \mathcal{Y}$ of a given type (`Ytype`), in such a way that $y = f(x)$ belongs to Y whenever $x \in X$. In Ada, such a bound F can be implemented by defining an appropriate `procedure F(X: in Xtype; Y: out Ytype)`. By definition, `X` belongs to the domain of `F` is no `Exception` is being raised.

Bounds on the basic operations involving the type `Ball` are defined in the package `Flts.Std.Balls`.

Using the definition (9.1) of a `CpCossin1`-type enclosure, it is clearly possible to implement a bound `Prod` on the map $(f, g) \mapsto f * g$ from $\mathcal{A} \times \mathcal{A}$ to $\mathcal{A}$. This and other basic bounds that include the type `CpCossin1` are defined in package `CpCossins1`. Bounds on basic operations for the types `Fourier1` and `LTaylor` are defined in packages `Fouriers1` and `LTaylors`, respectively.

The package `Cylinders` defines the type `Cylinder` as a `CpCossin1` with coefficients of type `Fourier1`. This determines our enclosures for the space $\mathcal{A}_\mathcal{B}$. Besides some general infrastructure related to quasi-Newton maps, most procedures in `Cylinders` are specific to the problem at hand. A rather trivial example is the bound `NegInvLap` on $-\Delta^{-1}$. Bounds on the operator L^q are implemented by the procedure `Lq`. It uses the estimates described in Sections 4 and 8. The procedures `Disk_Iso`, `Inv_Ellipse`, and `Cassini` construct `LTaylor`-type enclosures for the associated multiplication operators $u \mapsto |\psi'|^2 u$. They use the estimates in Propositions 5.1 (for $k = 1, 2$) and Proposition 5.2 via the procedures `PowerNegOne1` ($k = 1$), `PowerNegOne2` ($k = 2$), and `PowerNegThreeHalf`, respectively. The procedure `Apply` is a bound on the map $(\mathbb{L}, u) \mapsto \mathbb{L}u$ from $\mathcal{L}_\mathcal{B} \times \mathcal{A}_\mathcal{B}$ to $\mathcal{A}_\mathcal{B}$. Some other procedures in `Cylinders` are used to plot graphs and are not part of the proof.

`Cylinders` also defines the type `CylinderMode` that characterize subspaces like $\mathbb{P}_j \mathcal{A}_\mathcal{B}$ (coefficient modes) and $\mathbb{P}_{\ge j} \mathcal{A}_\mathcal{B}$ (error modes). Arrays of `CylinderMode` are used by the procedure `Make` to define partitions of unity (in the sense of direct sums) for the spaces $\mathcal{A}_j$ described in Section 7. This is the problem-specific part of a general infrastructure designed to implement bounds on quasi-Newton maps. Another part is handled by the

packages `Linear` and `Linear.Contr` that work with a generic type `Fun` and associated `Modes`. These two packages contain all the tools needed to construct (in terms of bounds) a quasi-Newton map $\mathcal{N}$ from a given map G, and to verify bounds like (7.2). The main task is to estimate the derivative of a linear operator such as $D\mathcal{N}(h)$. A description of how this is done by using `Modes` is given in [18,17].

The package at the top of our hierarchy is `Cylinders.Fix`. It first defines a bound `GMap` on the map G defined by (2.6), as well as a bound `DGMap` on the derivative of G. These are just compositions of bounds implemented in `Cylinder`. Then `Cylinders.Fix` instantiates the packages `Linear` and `Linear.Contr` with `Fun => Cylinder` and `Mode => CylinderMode`. Using the procedures `Op_Norm` and `DContr` from these two packages, implementing a bound `DContrNorm` on the map $h \mapsto \|D\mathcal{N}(h)\|$ is straightforward. This bound is used by `ContrFix` to verify the inequalities in the claim of Lemma 7.1. The ball B_δ that appears in this lemma has a representable radius $\delta > 0$ and is described by a `Cylinder`-type enclosure.

9.3. Organizing the bounds

The existence part in our proof of Lemma 7.1 is organized by the program `Run_All`. For each row in Table 1, `Run_All` reads the necessary parameter values from the package `Params`, and then calls the (standalone) procedures `Approx_Fixpt` and `Check_Fixpt` with an argument of type `Param`. Both of these procedures use an approximate fixed point $\bar{w}$ that is provided in a data file [20]. The procedure `Approx_Fixpt` is purely numerical and determines a matrix `M` that defines the operator M used in (7.1). Using the values in `Param`, the procedure `Check_Fixpt` instantiates the package `Cylinders.Fix` with the proper arguments. Then it calls `ContrFix` to verify the inequalities in the claim of Lemma 7.1.

The remaining claims in Lemma 7.1 are verified by the program `Run_Misc`, which runs `Check_Misc` for each choice of `Param`. The main procedures in `Check_Misc` are `Check_Min`, `Check_Max`, `Level_Stat`, and `Check_Injective`. The first two verify the ranges in column 9 of Table 1, using numerical data on extrema that has been generated by the program `Run_Num_Extrema`. The procedure `Level_Stat` generates extra level-set information that shows e.g. that the symmetries listed in columns 6 and 7 are maximal. For near-Cassini solutions, `Check_Injective` verifies the inequalities in Proposition 6.2. The approximate Morse index in the last row of Table 1 was obtained using the program `Approx_Morse`.

Our programs were run successfully on a standard desktop machine, using a public version of the gcc/gnat compiler [22]. Instructions on how to compile and run these programs can be found in the README file that is included with the source text [20].

10. Additional figures

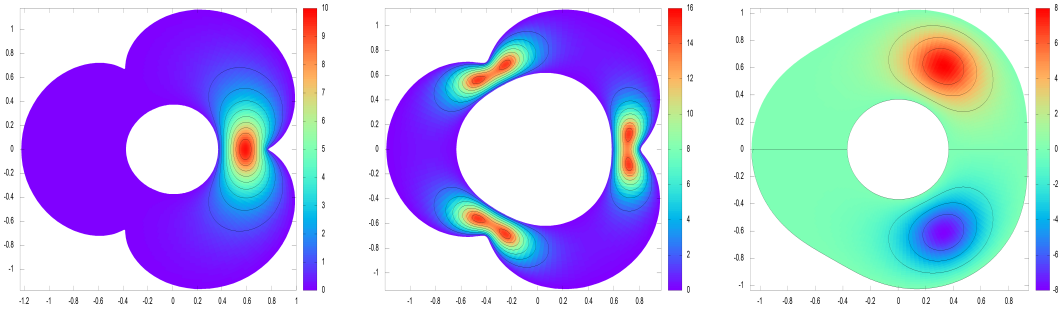

Figure 6. Domains and level sets for the solutions 5,6,7.

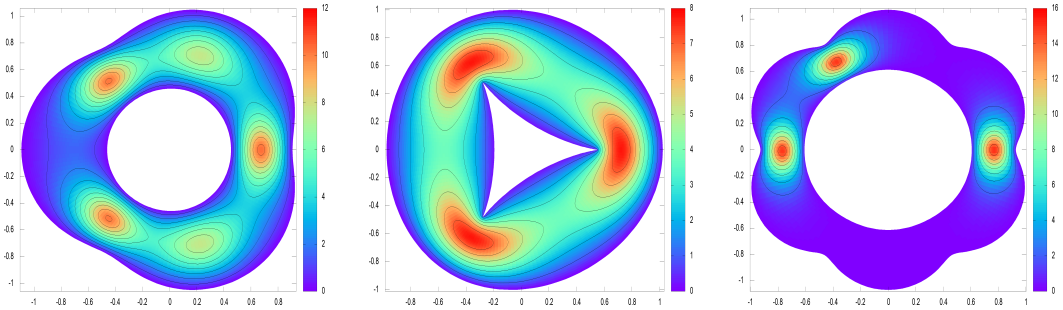

Figure 7. Domains and level sets for the solutions 8,9,10.

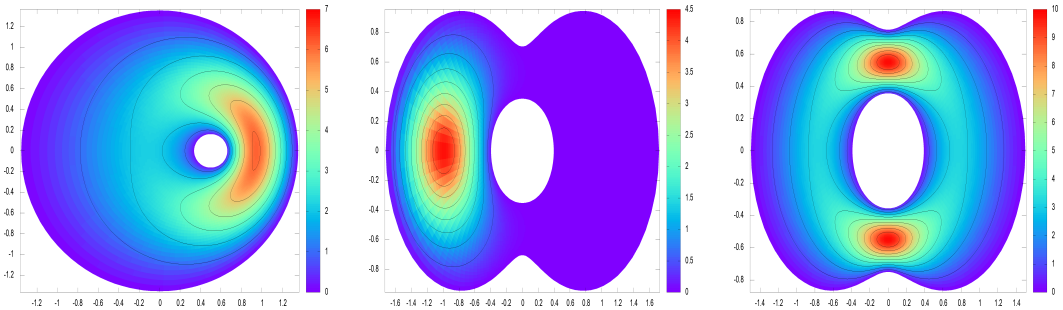

Figure 8. Domains and level sets for the solutions 13,14,15.

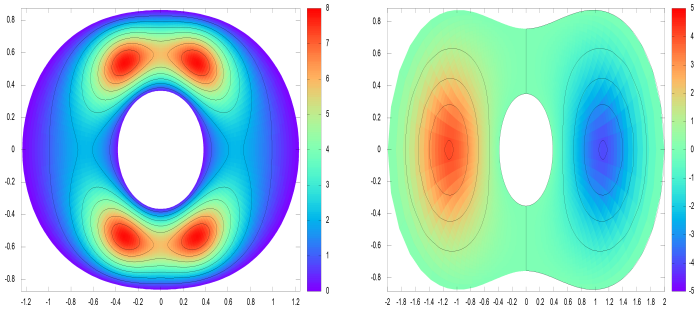

Figure 9. Domains and level sets for the solutions 16,17.

References

[1] A. Friedman, *On the regularity of the solutions of nonlinear elliptic and parabolic systems of partial differential equations*, J. Math. Mech. **7**, 43–59 (1958).

[2] C. Morrey, Jr. *On the analyticity of the solutions of analytic non-linear elliptic systems of partial differential equations. I. Analyticity in the interior*, Am. J. Math. **80**, 198–218 (1958).

[3] L.A. Segel, *Application of conformal mapping to viscous flow between moving circular cylinders*, Quart. Appl. Math. **18**, 335–353 (1961).

[4] A. Ambrosetti, P. Rabinowitz, *Dual variational methods in critical point theory and applications*, J. Funct. Anal. **14**, 349–381 (1973).

[5] C.V. Coffman, *A non-linear boundary value problem with many positive solutions*, J. Differ. Equations **54**, 429–437 (1984).

[6] Y.Y. Li, *Existence of many positive solutions of semilinear elliptic equations in annulus*, J. Differ. Equations **83**, 348–367 (1990).

[7] J. Byeon, *Existence of many nonequivalent nonradial positive solutions of semilinear elliptic equations on three-dimensional annuli*, J. Differ. Equ. **136**, 136–165 (1997).

[8] G. Chen, W.-M. Ni, J. Zhou, *Algorithms and visualization for solutions of nonlinear elliptic equations, Part I: Dirichlet Problem*, Int. J. Bifurc. Chaos **10**, 1565–1612 (2000).

[9] R. Kajikiya, *Orthogonal group invariant solutions of the Emden-Fowler equation*, Nonlin. Analysis **44**, 845–896 (2001).

[10] G. Chen, W-M. Ni, A. Porronnet, J. Zhou, *Algorithms and visualization for solutions of nonlinear elliptic equations, Part II: Dirichlet, Neumann and Robin boundary conditions and problems in 3D*, Int. J. Bifurc. Chaos **11**, 1781–1799 (2001).

[11] T. Bartsch, *Critical Point Theory on Partially Ordered Hilbert Spaces*, J. Funct. Anal. **186**, 117–152 (2001).

[12] M. Plum, *Computer-assisted proofs for semilinear elliptic boundary value problems*, Japan J. Indust. Appl. Math. **26**, 419–442 (2009).

[13] G. Arioli, H. Koch, *Non-symmetric low-index solutions for a symmetric boundary value problem*, J. Differ. Equations **252**, 448–458 (2012).

[14] G. Arioli, H. Koch, *Existence and stability of traveling pulse solutions of the FitzHugh-Nagumo equation*, Nonlin. Analysis **113**, 51–70 (2015).

[15] I. Balázs, J.B. van den Berg, J. Courtois, J. Dudás, J.-P. Lessard, A. Vörös-Kiss, J.F. Williams, X.Y. Yin, *Computer-assisted proofs for radially symmetric solutions of PDEs*, J. Comput. Dyn. **5**, 61–80 (2017).

[16] F. Pacella, M. Plum, D. Ruetters, *A computer-assisted existence proof for Emden's equation on an unbounded L-shaped domain*, Commun. Contemp. Math. **19**, 1750005 (2017).

[17] G. Arioli, H. Koch, *Non-radial solutions for some semilinear elliptic equations on the disk*, Nonlin. Analysis **179**, 294–308 (2019).

[18] G. Arioli, H. Koch, *Traveling wave solutions for the FPU chain: a constructive approach*, Nonlinearity **33**, 1705–1722 (2020).

[19] S. Blatt, *On the analyticity of solutions to non-linear elliptic partial differential systems*,

[20] G. Arioli, H. Koch. The source code for our programs, and data files, are available at web.ma.utexas.edu/users/koch/papers/annulus/

[21] Ada Reference Manual, ISO/IEC 8652:2012(E); see e.g. www.ada-auth.org/arm.html

[22] A free-software compiler for the Ada programming language, which is part of the GNU Compiler Collection; see e.g. gnu.org/software/gnat/

[23] The Institute of Electrical and Electronics Engineers, Inc., *IEEE Standard for Binary Floating–Point Arithmetic*, ANSI/IEEE Std 754–2008. doi:10.1109/IEEESTD.2008.4610935

[24] The MPFR library for multiple-precision floating-point computations with correct rounding; see e.g. www.mpfr.org/